Available online at www.sciencedirect.com
SCIENCE DIRECT
Journal of Catalysis 241 (2006) 378–388
JOURNAL OF CATALYSIS
www.elsevier.com/locate/jcat

Effect of Sn addition to $Pt/CeO_2–Al_2O_3$ and Pt/Al_2O_3 catalysts: An XPS, ^{119}Sn Mössbauer and microcalorimetry study

J.C. Serrano-Ruiz [a], G.W. Huber [b], M.A. Sánchez-Castillo [b], J.A. Dumesic [b], F. Rodríguez-Reinoso [a], A. Sepúlveda-Escribano [a,*]

[a] *Departamento de Química Inorgánica, Universidad de Alicante, Apartado 99, E-03080, Alicante, Spain*
[b] *Department of Chemical Engineering, University of Wisconsin-Madison, Madison, WI 53706, USA*

Received 22 February 2006; revised 4 May 2006; accepted 8 May 2006

Available online 12 June 2006

Abstract

The effect of adding Sn to $Pt/CeO_2–Al_2O_3$ and Pt/Al_2O_3 catalysts was studied with X-ray photoelectron spectroscopy (XPS), ^{119}Sn Mössbauer spectroscopy, and adsorption microcalorimetry of CO at room temperature. Catalysts were reduced in situ at 473 (non-SMSI state) and 773 K (SMSI state). ^{119}Sn Mössbauer and XPS results indicated that the presence of cerium in bimetallic catalysts inhibited reduction of tin, and that tin facilitated the reduction of cerium(IV) to cerium(III). Microcalorimetric analysis indicated that adding cerium caused the appearance of a more heterogeneous distribution of active sites, whereas adding tin led to a higher homogeneity of these sites. Reduction at 773 K decreased the Pt surface area as measured by CO chemisorption for all catalysts used in this study. Adding tin to Pt/Al_2O_3 and $Pt/CeO_2–Al_2O_3$ also decreased the Pt surface area due to formation of PtSn and possibly $Pt–SnO_x$ species. Adding cerium to Pt/Al_2O_3 caused a loss of Pt surface area only when the catalyst was reduced at 773 K, presumably due to migration of the reduced cerium onto Pt particles. Adding cerium to Pt/Al_2O_3 caused an increase in the catalytic activity for crotonaldehyde hydrogenation, whereas adding Sn to Pt/Al_2O_3 decreased the activity of Pt/Al_2O_3 catalysts. Higher reduction temperatures caused an increase in the initial catalytic activity for crotonaldehyde hydrogenation for all catalysts studied. Selectivity enhancements for crotyl alcohol formation in crotonaldehyde hydrogenation were observed for the Ce- and Sn-promoted catalysts after reduction at 773 K.

Keywords: Pt–Sn catalysts; CeO_2; Crotonaldehyde hydrogenation; Adsorption calorimetry; Mössbauer; XPS

1. Introduction

The effects of so-called strong metal–support interactions (SMSI) have received considerable attention ever since the original discovery by Tauster et al. [1]. These effects induced by high-temperature reduction treatments (typically $T_{redn} \geqslant 723$ K) are generally considered associated with reducible supports, such as TiO_2 [2], NbO_5 [3], and especially CeO_2 [4,5]. Catalysts supported on reducible oxides have shown interesting catalytic and chemisorption properties, including decreased H_2 chemisorption ability [6], suppressed alkane hydrolysis activity, increased CO hydrogenation activity [7], and improved selectivity of crotyl alcohol for crotonaldehyde hydrogenation [8–10] when catalysts are subjected to high-temperature reduction (>773 K). Electron microscopy studies have shown that after high-temperature reduction, partially reduced oxide species migrate and decorate the metal surface [4–6,11,12]. Bernal et al. have shown that for a Pt/CeO_2 catalyst, this decoration occurs at a reduction temperature of 973 K and $CePt_5$ particles are formed at temperatures of 1173 K [13]. This decoration effect occurs at lower temperatures for metal/TiO_2 systems. Datye et al. have postulated that the SMSI effect is different for metal/TiO_2 and metal/CeO_2 systems [7]; using HRTEM, they observed that Pt clusters grew in an epitaxial relation on CeO_2, whereas reduced TiO_2 particles migrated onto Pt clusters when catalysts were reduced at 773 K. This result was confirmed by Abid et al., who also observed that Pt particles 3–4 nm in size grew in an epitaxial pattern on ceria after reduction at 773 K [14]. Thus, CeO_x is able to modify the geometric properties of Pt [14].

* Corresponding author. Fax: +34 965 90 34 54.
E-mail address: asepul@ua.es (A. Sepúlveda-Escribano).

0021-9517/$ – see front matter
doi:10.1016/j.jcat.2006.05.005

The existence of metal–support interactions can be assessed with the help of probe reactions such as hydrogenation reactions, for which both the activity and the selectivity are generally dependent on the catalyst reduction. One of the most interesting reactions is the hydrogenation of α,β-unsaturated aldehydes [8,9]. This reaction can produce saturated aldehyde (through hydrogenation of the C=C bond) or unsaturated alcohol (through hydrogenation of the carbonyl C=O bond). The former reaction is favored on unpromoted platinum catalysts from both thermodynamic and kinetic points of view. However, the use of reducible supports such as CeO_2 produces an important enhancement in the selectivity toward the unsaturated alcohols [10,14]. For example, Englisch et al. [41] observed that TiO_x species migrated onto Pt particles after high-temperature reduction (773 K), leading to improved catalyst activity and selectivity toward crotyl alcohol in crotonaldehyde hydrogenation. They concluded that this increase in activity was probably due to crotonaldehyde adsorption at interfacial Pt–TiO_x sites.

The hydrogenation of crotonaldehyde on Pt has been shown to be structure-sensitive, where the selectivity and activity is a function of Pt metal particle size [41]. Theoretical [42] and single-crystal studies [47] indicate that the adsorption structures of α,β-unsaturated aldehydes depend on the metal surface planes. Beccat et al. showed that Pt(111) exhibits some selectivity to crotyl alcohol, whereas the other low-index Pt surface did not make any crotyl alcohol [47]. Englisch et al. concluded that increasing the abundance of Pt(111) surfaces in a catalyst can increase the selectivity to crotyl alcohol [41].

The addition of a second metal to noble metal catalysts can modify catalytic behavior, such as in the case of bimetallic Pt–Sn catalysts used for dehydrogenation processes [15,16] or for hydrogenation of α,β-unsaturated aldehydes [17]. Adding tin to Pt catalysts has been shown to improve the selectivity of crotyl alcohol for crotonaldehyde hydrogenation [18,19].

Despite the large amount of research devoted to the SMSI effect, very few studies have reported the effect of adding a second, nonactive metal to catalysts supported on reducible oxides. In these complex systems, the role of the reducible oxide in determining the chemical nature of the second metal species is particularly important, because it determines the degree and type of interactions that can occur with the noble metal, thus conditioning its catalytic properties in numerous interesting reactions (e.g., selective hydrogenations, alkane dehydrogenation).

In this paper we report a pioneer study on the presence of two promoters—tin and ceria—in Pt-based catalysts, and the effect of reciprocal interactions between these species have been followed by a great number of characterization techniques. The main objective was to analyze the effect of reduction temperature on Pt/CeO_2–Al_2O_3 catalysts and to analyze how catalytic properties change with the presence of a second, nonactive metal (e.g., Sn) in a given Pt/Sn atomic ratio. Various techniques (XPS, adsorption microcalorimetry, and Mössbauer spectroscopy) were used to characterize catalysts reduced at 473 K (non-SMSI state) and 773 K (SMSI state) to study this effect. In addition, hydrogenation of crotonaldehyde was used as a probe reaction to complete the results obtained in the characterization section. To the best of our knowledge, this is the first time that so comprehensive a study on this type of system has been reported.

2. Experimental

2.1. Catalyst preparation

The starting support was a commercial γ-Al_2O_3 (Puralox SCCa 150/200; SASOL), with a BET surface area of 228 $m^2\,g^{-1}$ (N_2, 77 K). The CeO_2–Al_2O_3 support was prepared by impregnating the γ-Al_2O_3 with an aqueous solution of $Ce(NO_3)_3{\cdot}6H_2O$ (Aldrich, 99%) of the appropriate concentration to load 25 wt% CeO_2 (5 mL of solution per g of γ-Al_2O_3). The slurry thus formed was stirred at room temperature for 24 h, and the excess solvent was removed by heating at 353 K for 2 h. The solid thus obtained was dried overnight at 383 K, followed by calcination at 673 K for 6 h, at a heating rate of 2 K min^{-1}. The CeO_2–Al_2O_3 support had a BET surface area of 153 $m^2\,g^{-1}$ (N_2, 77 K).

The monometallic catalysts, Pt/Al_2O_3 and Pt/CeO_2–Al_2O_3, were prepared by impregnating the supports with aqueous solutions of $[Pt(NH_3)_4](NO_3)_2$ (Aldrich, 99%). The solids were dried overnight at 383 K and then calcined in air at 673 K for 6 h. The bimetallic catalysts, Pt–Sn/Al_2O_3 and Pt–Sn/CeO_2–Al_2O_3, were prepared by successive impregnation. First, the supports were impregnated with aqueous nitric acid solutions of $Sn(C_2O_4)$ (from Aldrich, 98%), and then the samples were dried at 383 K and calcined at 673 K for 6 h. Platinum was subsequently added to the supports following the aforementioned procedure. The amount of tin loaded corresponded to an atomic Pt/Sn ratio of 1:1. The actual metal content of the catalysts was determined by ICP measurements as reported in Table 1.

2.2. Catalyst characterization

X-ray photoelectron spectra (XPS) were acquired with a VG-Microtech Multilab 3000 spectrometer equipped with a hemispherical electron analyzer and a Mg$K\alpha$ ($h = 1253.65$ eV; 1 eV $= 1.6302 \times 10^{-19}$ J), 300-W X-ray source. The powder samples were pressed into small Inox cylinders and then mounted on a sample rod placed in a pretreatment chamber and reduced in flowing H_2 for 1 h at 473 and 773 K before being transferred to the analysis chamber. Before recording the spectra, the sample was maintained in the analysis chamber until a residual pressure of ca. 5×10^{-7} N m^2 was reached. The

Table 1
Summary of catalysts composition

Catalyst	Pt loading (wt%)	Sn loading (wt%)	Pt/Sn atomic ratio
Pt/Al_2O_3	1.88	–	–
Pt–Sn/Al_2O_3	1.77	1.44	0.74
Pt/CeO_2–Al_2O_3	1.43	–	–
Pt–Sn/CeO_2–Al_2O_3	1.43	1.19	0.73

spectra were collected at a pass energy of 50 eV. The intensities were estimated by calculating the integral of each peak, after subtracting the S-shaped background, and fitting the experimental curve to a combination of Lorentzian (30%) and Gaussian (70%) lines. All binding energies were referenced to the C 1s line at 284.6 eV, which provided binding energy (BE) values with an accuracy of ±0.2 eV.

Room temperature Mössbauer spectra of ^{119}Sn were collected using an Austin Science Associates model S-600 Mössbauer spectrometer connected to a microcomputer with a PCAII data collection board. The spectrometer was operated in the constant-acceleration mode, with a 10-mCi single-line γ-ray source of $Ca^{119m}SnO_3$ (Amarsham). Detection of the 23.88-keV γ-rays was achieved with a Xe–CO_2 proportional counter. A 0.05-mm-thick Pd foil was placed between the source and detector to filter 25.04- and 25.27-keV X-rays from the source. A 50/50 mixture of $BaSnO_3$ and β-Sn powder was used to calibrate the magnitude and linearity of the Doppler velocity for our system. Chemical shifts are reported relative to $BaSnO_3$ at room temperature. The catalysts were reduced at 473 and 773 K before collecting the spectra using hydrogen (Liquid Carbonic) purified by passing through a bed of molecular sieves (13X) at 77 K for 5 h.

Differential heats of CO adsorption were measured at 300 K in a Setaram BT2.15D heat-flux calorimeter as described in detail elsewhere [20]. This calorimeter was connected to a high-vacuum (base pressure $<10^{-6}$ Torr) volumetric system using Baratron capacitance manometers for precision pressure measurement ($\pm 0.5 \times 10^{-4}$ Torr). The maximum apparent leak rate of the volumetric system (including the calorimetric cells) was 10^{-6} Torr min^{-1} in a system volume of approximately 70 cm^3 (i.e., 10^{-6} μmol min^{-1}). The procedure for microcalorimetric measurements used in this study is described below: each sample (about 0.25 g) was treated ex situ in ultrapure hydrogen (99.999% with further purification, AGA) for 5 h (2 K min^{-1} ramp, 100 ml min^{-1}) at the desired temperature (473 or 773 K), after which the sample was purged for 1 h at the same temperature in ultra-high-purity helium (99.999% with further purification, AGA) to remove adsorbed hydrogen. Then it was sealed in a Pyrex NMR tube capsule and broken in a special calorimetric cell [20] once the sample had attained thermal equilibrium with the calorimeter. After the capsule was broken, the microcalorimetric data were collected by sequentially introducing small doses (1–10 μmol) of CO (99.5% with further purification, AGA) onto the sample until it became saturated. The resulting heat response for each dose was recorded as a function of time and integrated to determine the energy released (mJ). The amount of gas adsorbed (μmol) was determined volumetrically from the dose, equilibrium pressures, and system volumes and temperatures. The time required for the pressure to equilibrate in the calorimeter after each dose was approximately 1–15 min, and the heat response was monitored for 20–30 min after each dose to ensure that all heat was detected and to allow the heat response to return to the baseline value. The differential heat (kJ mol^{-1}), defined as the negative of the enthalpy change of adsorption per mole of gas adsorbed, was then calculated for each dose by dividing the heat released by the amount adsorbed.

The catalytic behavior of the samples in the vapor-phase hydrogenation of crotonaldehyde (2-butenal) was tested in a U-shaped quartz microflow reactor at atmospheric pressure under differential conditions. Before each reaction run, the catalyst (around 0.15 g) was reduced in situ at 473 and 773 K under flowing hydrogen (50 cm^3 min^{-1}) for 5 h and then cooled under hydrogen to the reaction temperature, 353 K. Then it was contacted with a reaction mixture (total flow, 50 cm^3 min^{-1}; H_2/CROALD ratio, 26) containing purified hydrogen and crotonaldehyde (Fluka, 99.5%) prepared by passing a hydrogen flow through a thermostabilized saturator (293 K) containing the unsaturated aldehyde. The concentration of the reactants and the products at the outlet of the reactor was determined by online gas chromatography with a Carbowax 20 M 58/90 semicapillary column.

3. Results and discussion

3.1. X-ray photoelectronic spectroscopy

The chemical species present on the catalysts surfaces and their proportions were evaluated by XPS. The energy regions of Ce 3d, Sn $3d_{5/2}$, and Pt $4d_{5/2}$ core levels in calcined and reduced (at 473 and 773 K) samples were recorded. Although the most intense photoemission lines of platinum were those arising from the Pt 4f levels, this energy region was overshadowed by the presence of a very strong Al 2p peak, and thus the Pt 4d lines were analyzed instead [21,22]. The fresh calcined samples showed an asymmetric broad Pt $4d_{5/2}$ peak (Fig. 1) that could be resolved, after curve fitting procedures, into three components with binding energies of 317.9–318.7, 316.1–316.8, and 314.3–314.8 eV. The two components at higher binding energies can be ascribed to PtO_2 species [23,24] created after the calcination process, whereas the third band at lower binding

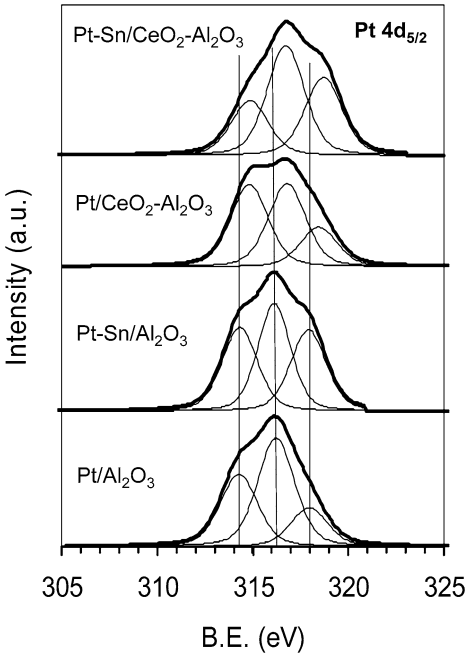

Fig. 1. XPS Pt $4d_{5/2}$ spectra of the calcined (unreduced) catalyst.

energies can be assigned to the presence of Pt(II) species. This assignment of the Pt oxidation state is difficult, and data in the literature are contradictory. Furthermore, the low levels of Pt present in the samples, along with the broad nature of the Pt 4d features, introduce considerable uncertainty in the determination of binding energies. It is interesting to observe that the Pt $4d_{5/2}$ BE values of the samples containing ceria are shifted to higher values (Fig. 1). The observed shift in binding energies may be the consequence of interaction with the cerium phase, leading to electronic polarization of the platinum precursor clusters. This result is not in agreement with the work of Navarro et al. [22], who reported a shift to lower binding energies in cerium-containing platinum catalysts. However, it has been found that this shift in BE created by the interaction of platinum particles with ceria is strongly dependent on the cerium content of the catalysts [25]. Thus, catalysts with high cerium content (as in the present study) show higher Pt $4d_{5/2}$ BE, whereas platinum particles in catalysts with low cerium content seem to be slightly more reduced than in the corresponding cerium-free counterpart [25].

The chemical changes in the platinum particles after reduction in H_2 at 473 and 773 K were also investigated by XPS. Fig. 2 shows, as a representative sample, the Pt $4d_{5/2}$ spectra for the calcined and the reduced samples for the $Pt/CeO_2–Al_2O_3$ catalyst. Table 2 gives the Pt $4d_{5/2}$ BEs for all of the catalysts under study, with the corresponding contribution to the overall signal in parentheses. The XPS spectra indicate a shift of the Pt $4d_{5/2}$ BEs toward lower values with increasing reduction temperature. It is interesting to observe the appearance of a band centered at around 313.0 eV in reduced samples, which is indicative of the presence of Pt^0 species, in agreement with results of Shyu et al. [23]. It should be noted that in all catalysts studied, even after reduction at 773 K, platinum seems to maintain some δ^+ character [or even remain as oxidized Pt(II) species] indicating a strong platinum–support interaction.

The Sn $3d_{5/2}$ spectra for the fresh and reduced in situ catalysts are compared in Fig. 3. XPS spectra indicate a shift of the Sn $3d_{5/2}$ BE toward lower values with increasing reduction temperature in both cases, which is indicative of tin reduction. The results for the cerium-free $Pt–Sn/Al_2O_3$ catalyst (Fig. 3a) showed one asymmetric spectrum, probably due to the sum of two different contributions [Sn^{ox}(II and IV) and Sn(0)] to the overall signal. In the case of the unreduced catalyst, one small band appeared at 485.2 eV that may be ascribed to Sn(II) species, although most of the tin contribution was due to one band centered at 486.8 eV, characteristic of Sn(IV). The weight of this band at high BE in the overall signal decreased with reduction temperature, and one peak appeared centered at 484.7 eV. This contribution has been ascribed in the literature to reduced Sn^0 [17,26]. The intensity of this peak increased with reduction temperature (from 8 to 18% of the overall signal), indicating a higher amount of metallic tin after reduction at high temperature. However, the reduction of tin was not complete, and oxidized tin species were detected even after reduction at 773 K, in agreement with previous results on alumina-supported catalysts [27–29]. Discriminating between

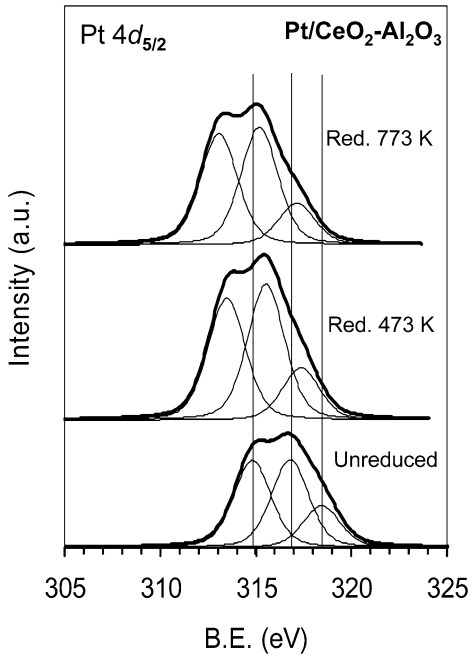

Fig. 2. XPS Pt $4d_{5/2}$ spectra of the calcined (unreduced) and reduced $Pt/CeO_2–Al_2O_3$ catalyst.

Table 2
Catalysts characterization by XPS

Catalyst	Red. temperature (K)	Pt/Al	BE Pt $4d_{5/2}$ (eV)	Pt/Sn	Pt/Ce	Ce/Al	%Ce(III)
Pt/Al_2O_3	Unreduced	0.0038	314.3(33), 316.2(49), 317.9(18)	–	–	–	
	473	0.0037	313.0(34), 315.2(45), 317.0(21)	–	–	–	
	773	0.0038	313.0(36), 315.2(45), 317.0(19)	–	–	–	
$Pt–Sn/Al_2O_3$	Unreduced	0.0045	314.3(32), 316.1(38), 317.9(30)	0.32	–	–	
	473	0.0041	313.5(29), 315.4(42), 317.3(29)	0.29	–	–	
	773	0.0032	313.0(32), 314.8(39), 316.4(29)	0.13	–	–	
$Pt/CeO_2–Al_2O_3$	Unreduced	0.0044	314.8(40), 316.8(41), 318.5(19)	–	0.67	0.0066	20
	473	0.0043	313.5(39), 315.5(44), 317.4(17)	–	0.49	0.0087	37
	773	0.0037	313.1(41), 315.2(43), 317.1(16)	–	0.30	0.0124	39
$Pt–Sn/CeO_2–Al_2O_3$	Unreduced	0.0047	314.8(23), 316.7(45), 318.7(32)	1.33	2.68	0.0017	33
	473	0.0032	313.5(28), 315.4(46), 317.4(26)	0.80	1.61	0.0020	38
	773	0.0037	313.0(33), 315.0(43), 316.8(24)	0.49	1.35	0.0027	46

Sn(II) and Sn(IV) with XPS is difficult. The objective of the deconvolution was mainly to separate the contribution of oxidized tin species [both Sn(II) and Sn(IV)] from the contribution of metallic tin. It has been found that the Sn^{ox}/Sn_{total} ratio depends on, among other factors, the type of support [27]. When silica or carbon are used as the catalyst support, their inertness favors the interaction between platinum and tin, making it possible to achieve reduction of Sn particles at moderate temperatures [16,19,30,31]. When alumina is used as a support, it interacts strongly with the Sn and hinders the reduction of SnO [32–34].

The spectra obtained with the cerium-containing bimetallic catalyst Pt–Sn/CeO_2–Al_2O_3 (Fig. 3b) had a Gaussian shape. After calcination and reduction at 473 K, no reduced tin species were detected (Fig. 3b). In contrast, the cerium-free catalysts contained a small amount of reduced Sn (8%) after reduction at 473 K. Only after reduction at high temperature (773 K) did Sn^0 (centered at 484.4 eV) appear for the Pt–Sn/CeO_2–Al_2O_3 catalyst. The reduced Sn species had a weight contribution of 16% of the Sn species, slightly lower than that in the cerium-free catalyst (18%). As noted above, the extent of tin reduction depends strongly on the support. It seems that the presence of cerium modified the Sn–alumina interaction, stabilizing the oxidized tin species. In this way, Del Angel et al. [35] modified Pt–Sn/Al_2O_3 catalysts with the reducible oxide La_2O_3 and observed a decrease in the amount of metallic tin with increasing La content for catalysts reduced at 573 K.

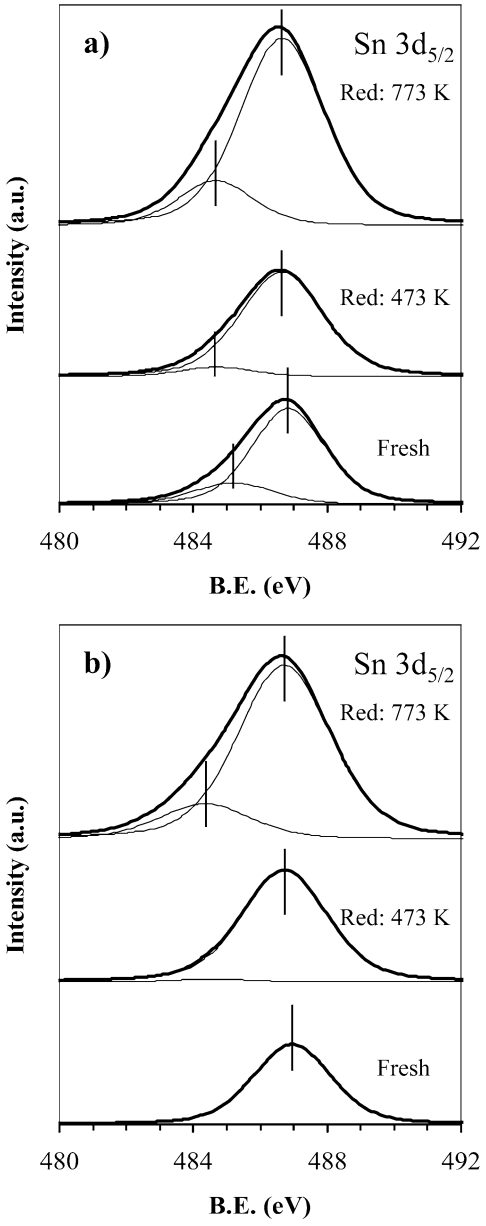

Fig. 3. XPS Sn $3d_{5/2}$ spectra of the calcined (unreduced) and reduced catalysts. (a) Pt–Sn/Al_2O_3; (b) Pt–Sn/CeO_2–Al_2O_3.

Cerium 3d XPS spectra were analyzed for Pt/CeO_2–Al_2O_3 and Pt–Sn/CeO_2–Al_2O_3 catalysts both after calcination and after in situ reduction at 473 and 773 K. This complex spectrum (not shown) was analyzed by fitting two sets of spin multiplets, corresponding to the $3d_{3/2}$ and $3d_{5/2}$ contributions, labeled u and v, respectively, and using up to four peaks from each contribution [36]. The percentages of CeO_2 reduction after the different treatments were determined taking into consideration the relative intensity of the peaks representative of Ce(III) in the total Ce 3d region [9]. The values obtained are plotted in Fig. 4 and reported in Table 2. It can be seen that the extent of Ce(IV) reduction increased with reduction temperature. There was a certain amount of Ce(III) even in the fresh (calcined) catalysts, probably due to photoreduction of Ce(IV) ions during XPS experiments, as also reported by Mastelaro et al. [37]. The extent of Ce(IV) reduction was greater for the bimetallic catalyst at the two reduction temperatures used in this work. This result indicates that, as seen in the Sn XPS spectra, Sn and Ce were interacting. After reduction at 473 K, both catalysts showed similar levels of cerium reduction (around 38%); however, when catalysts were reduced at 773 K, the bimetallic catalyst showed a higher amount of reduced cerium (46%) than its monometallic counterpart (39%). This effect of second metal in cerium reducibility has been observed before for Pt–Zn/CeO_2–SiO_2 catalysts [9]. It seems that the presence of tin facilitates H_2 transport from the platinum surface to the ceria support.

Table 2 shows that the Pt/Al XPS atomic ratio (which can be considered a measure of the platinum dispersion on the support)

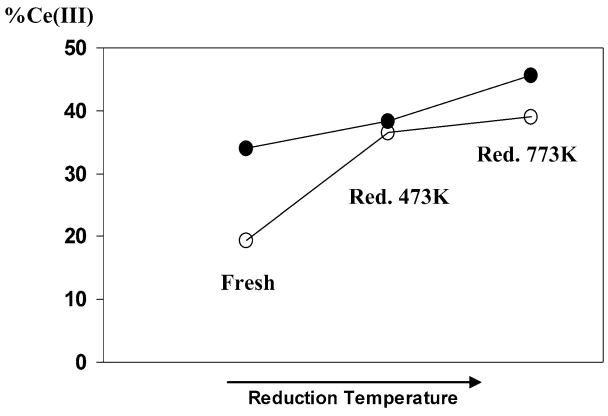

Fig. 4. %Ce(III) as a function of the reduction temperature: (○) Pt/CeO_2–Al_2O_3; (●) Pt–Sn/CeO_2–Al_2O_3.

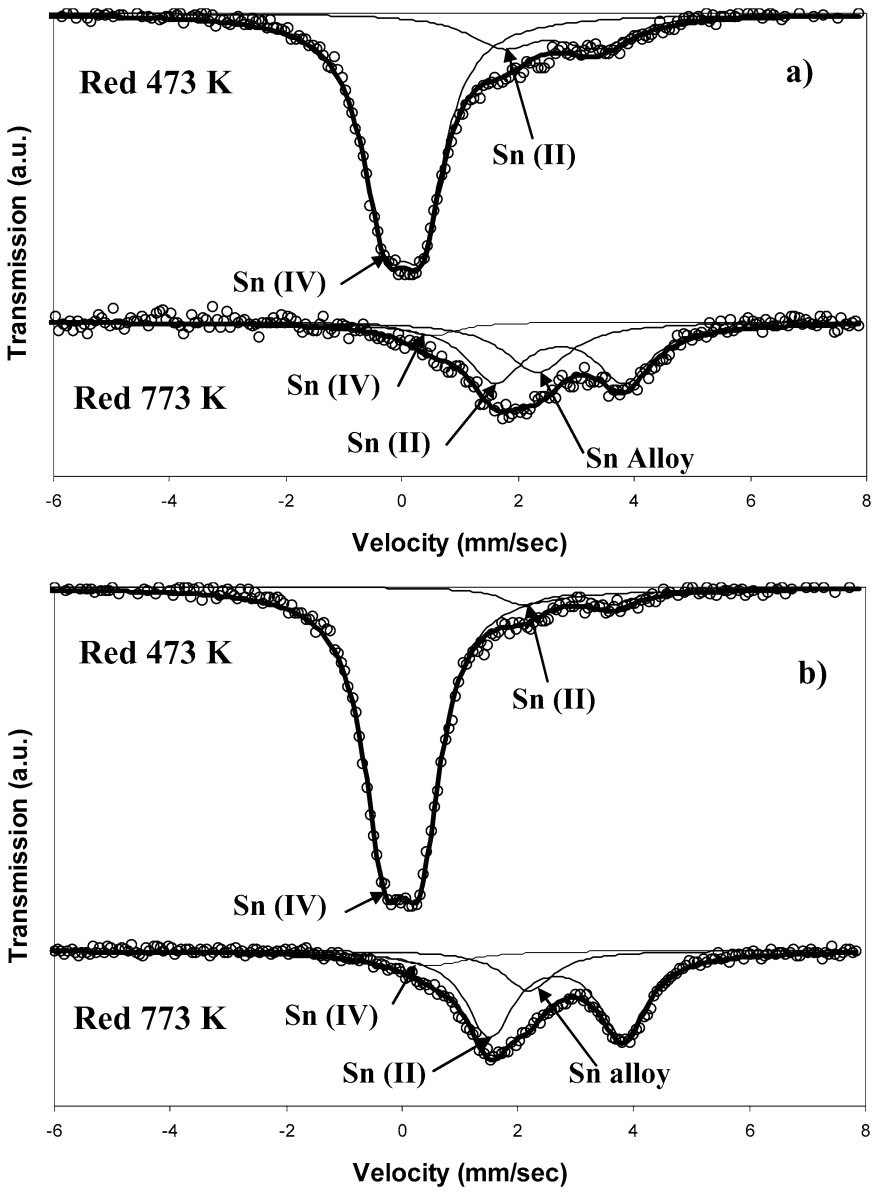

Fig. 5. ^{119}Sn Mössbauer spectra for (a) Pt–Sn/Al_2O_3 and (b) Pt–Sn/CeO_2–Al_2O_3 catalysts after reduction at 473 and 773 K.

decreased with reduction temperature for all catalysts prepared except Pt/Al_2O_3. Thus, platinum did not sinter appreciably after reduction treatment. For Pt–Sn/Al_2O_3, the observed decrease in Pt/Al atomic ratio was accompanied by a decrease in Pt/Sn values. As the reduction temperature was increased, the tin decreased the platinum surface area by forming an alloy or by covering with oxidized tin species for the Pt–Sn/Al_2O_3 catalyst. Increasing the reduction temperature decreased the Pt/Ce atomic ratio and increased the Ce/Al atomic ratio for the Pt/CeO_2–Al_2O_3 catalyst. This result suggests that during reduction, the cerium ions can migrate onto platinum particles, which could account for the decreased Pt/Al atomic ratio in monometallic Pt/CeO_2–Al_2O_3 catalyst. Pt–Sn/CeO_2–Al_2O_3 showed lower Ce/Al atomic ratios than the monometallic counterpart. This behavior again can be attributed to the coverage of ceria (or partially reduced ceria) particles by oxidized tin species with a strong interaction with the support.

3.2. Tin Mössbauer spectroscopy

The oxidation state of Sn as a function of reduction temperature was studied in more detail by ^{119}Sn Mössbauer spectroscopy. Fig. 5 shows the room temperature spectra for bimetallic catalysts after reduction at 473 and 773 K. The fitting parameters of these spectra are shown in Table 3. The Pt–Sn/Al_2O_3 (Fig. 5a) spectrum after reduction at 473 K showed one small doublet characteristic of Sn^{2+} (20% area) and one large band (80% area) at an isomer shift of 0 mm s^{-1}, typical of Sn^{4+} species. After reduction at 773 K, the Sn^{4+} species decreased (7% area), whereas the relative area due to Sn^{2+} increased from 20 to 62%. It should be noted that the chemical composition of the Sn species is not strictly proportional to the relative area in the Mössbauer spectra because of differences in the recoil-free fractions. The high-temperature reduction treatment also resulted in the appearance of a singlet peak (31% area) at an

Table 3
^{119}Sn Mössbauer parameters of Pt–Sn catalysts at 300 K

Catalyst	Reduction temperature (K)	Isomer shift (mm s^{-1})	Quadrupole splitting (mm s^{-1})	Relative area (%)	Chemical form of Sn	Average Sn state
Pt–Sn/Al_2O_3	473	0.03	0.63	80	Sn(IV)	3.6
		2.55	1.60	20	Sn(II)	
	773	2.33	0.00	31	Pt–Sn alloy	1.5
		2.71	2.22	62	Sn(II)	
		0.50	0.00	7	Sn(IV)	
Pt–Sn/CeO_2–Al_2O_3	473	0.00	0.60	93	Sn(IV)	3.9
		2.87	1.56	7	Sn(II)	
	773	2.19	0.00	21	Pt–Sn alloy	1.7
		2.67	2.30	71	Sn(II)	
		0.50	0.00	8	Sn(IV)	

isomer shift of 2.33 mm s^{-1}, which can be assigned to metallic tin alloyed with platinum [16]. These results are consistent with the XPS results, indicating that high-temperature reduction is needed to reduce the Sn species. The Sn^{2+} species could be an Sn species interacting with alumina.

The spectrum for Pt–Sn/CeO_2–Al_2O_3 (Fig. 5b) reduced at 473 K was similar to that of the cerium-free catalyst, although in this case, more Sn^{4+} was detected (93%). After the treatment at high temperature (773 K), the spectrum consisted principally of Sn^{2+} (69%) and a lesser amount of metallic tin (21%). The average oxidation state of tin was higher than in the cerium-free catalyst (1.7 vs. 1.5). In this case, the Sn^{2+} species could be interacting with both alumina and ceria. These results are consistent with XPS measurements showing that reduction of oxidized tin species is more difficult when cerium is present on the alumina support. The XPS and Mössbauer data indicate that Sn is both oxidized and reduced; therefore, the catalyst would be expected to contain a complicated mixture of Pt–Sn, Pt–CeO_x, and Pt–SnO_x sites at the surface.

3.3. CO adsorption microcalorimetry

Figs. 6 and 7 show the differential heat of CO adsorption versus coverage at 298 K for catalysts reduced at 473 and 773 K. As the CO coverage increased, the differential heat of adsorption decreased due to adsorption on weaker sites and/or interactions between adsorbed species. At higher coverage, the significant decrease in the differential heat of adsorption indicates saturation of the surface. For Pt/Al_2O_3 (Fig. 6a), the initial differential heat was 140 kJ mol^{-1} for the catalyst reduced at 473 K, in good agreement with other studies of CO adsorption on alumina-supported platinum catalysts [38]. Adsorption heat decreased to a coverage of 20 μmol CO g^{-1}, at which a plateau around 120 kJ mol^{-1} was observed. Reduction at higher temperature caused a decrease in initial heat (from 140 to 120 kJ mol^{-1}), which was maintained over a wide range of surface coverage before a drastic drop to the weakly adsorbed CO (70 kJ mol^{-1}). This finding indicates a higher homogeneity of the surface metal atoms for CO adsorption when catalyst is reduced at 773 K, with the higher initial heat of adsorption obtained in the sample reduced at low temperature attributed to the interaction of CO with highly unsaturated metal atoms at corners and edges [38]. Reduction at higher temperatures decreased the CO saturation coverage from 55 to 45 μmol CO g^{-1}, as reported in Table 4. This effect could be due to sintering of the Pt particles after high-temperature reduction, and this change was not observed with XPS.

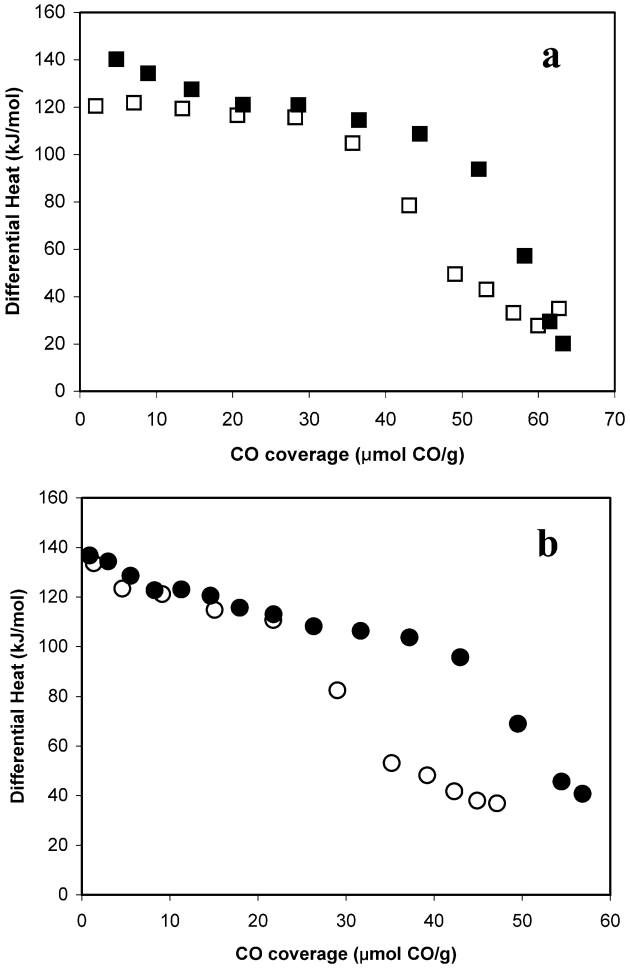

Fig. 6. Differential heats of carbon monoxide adsorption at 298 K on (a) Pt/Al_2O_3 and (b) Pt–Sn/Al_2O_3 catalysts after reduction at 473 K (■, ●) or 773 K (□, ○).

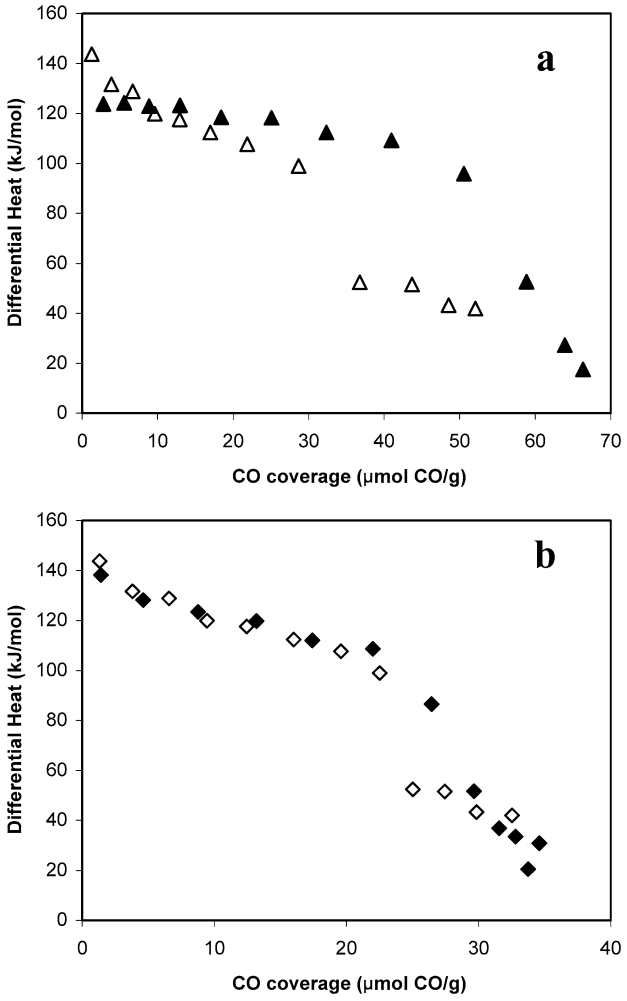

Fig. 7. Differential heats of carbon monoxide adsorption at 298 K on (a) Pt/CeO_2–Al_2O_3 and (b) Pt–Sn/CeO_2–Al_2O_3 catalysts after reduction at 473 K (▲, ◆) or 773 K (△, ◇).

Table 4
CO uptake and CO/Pt ratios for catalysts reduced at both 473 and 773 K

Catalyst	Reductuction temperature (K)	CO uptake (μmol CO g^{-1})	CO/Pt
Pt/Al_2O_3	473	55	0.57
	773	45	0.47
Pt–Sn/Al_2O_3	473	49	0.54
	773	32	0.35
Pt/CeO_2–Al_2O_3	473	55	0.75
	773	33	0.45
Pt–Sn/CeO_2–Al_2O_3	473	27	0.37
	773	24	0.33

No change in the initial heats (140 kJ mol^{-1}) was observed for the Pt–Sn/Al_2O_3 (Fig. 6b) catalyst after reduction at 773 K, probably because active sites placed in corners and edges were already covered by tin after reduction at low temperature. The adsorption heat-coverage profile was similar for the catalysts reduced at 473 and 773 K to about 20 μmol CO g^{-1}. However, reduction at 773 K caused a strong decrease in the saturation coverage value from 49 to 32 μmol CO g^{-1} (also detected by XPS), in agreement with other Pt–Sn (1:1) microcalorimetric studies [15,23,39]. Because Mössbauer results indicate the presence of Pt–Sn alloy after reduction at 773 K, changes in the initial heats of adsorption of CO on platinum could be expected. However, it has been shown that Pt–Sn catalysts prepared by sequential impregnation techniques can lead to a large fraction of unalloyed platinum [40]. In addition, an observable change in the initial heats of adsorption requires a larger fraction of Pt–Sn alloy formation [15].

Pt/CeO_2–Al_2O_3 (Fig. 7a) showed higher initial heats (from 123 to 143 kJ mol^{-1}) and lower CO saturation coverage (from 55 to 33 μmol CO g^{-1}; Table 4) when reduced at high temperature. In addition, the differential heat of CO adsorption strongly decreases with coverage, indicating a heterogeneous distribution of adsorption sites. This behavior could be due to decoration of the Pt metal with reduced ceria oxide (CeO_x). This decoration effect could also explain the inhibition of the chemisorption capacity of platinum detected by microcalorimetry and the XPS results for Pt/Al and Pt/Ce. This geometric effect would reduce the number of accessible platinum particles but at the same time produce new Pt–CeO_x sites at the metal–support interface [4]. As discussed by Bernal et al. [4], decoration of ceria usually occurs at higher reduction temperature (973 K) than that used here for Pt/CeO_2 catalysts. However, these results are based on catalysts supported on ceria instead of on ceria-supported alumina. It is interesting to note (Table 4) that cerium addition produced an increase in the CO/Pt ratio after reduction at 473 K (from 0.57 in Pt/Al_2O_3 to 0.75 in Pt/CeO_2–Al_2O_3); this could be due to the additional adsorption of CO on ceria, leading to greater amounts of adsorbed CO.

Pt–Sn/CeO_2–Al_2O_3 (Fig. 7b) showed similar heat-coverage profiles at both reduction temperatures. The saturation coverage decreased slightly from 27 to 24 μmol CO g^{-1} (Table 4) as the reduction temperature increased from 473 to 773 K. Note that the addition of both Sn and CeO_2 decreased the number of Pt surface sites. When only Sn or CeO_2 was added to Pt, a high temperature reduction was needed to cause a decrease in Pt surface area; however, when both Sn and CeO_2 were added to the catalyst, a synergistic effect was seen in which the Pt surface area was significantly lower at a reduction temperature of 473 K. This effect was probably due to the ability of Sn to increase the reducibility of CeO_2, thus causing the decoration effect at a lower reduction temperature.

3.4. Catalytic behavior

The performance of the catalysts was tested for the hydrogenation of crotonaldehyde. The behavior was similar in all cases; after the first stages of reaction (approximately 25 min on stream), the activity decreased to a stable value that was similar for all catalysts. The deactivation of the catalyst has been attributed to decarbonylation of the reactant molecule yielding carbon monoxide, which is irreversibly adsorbed on platinum at the reaction conditions [41]. Although no appreciable differences were found in steady-state activities for the different catalysts, interesting results were obtained in initial activities.

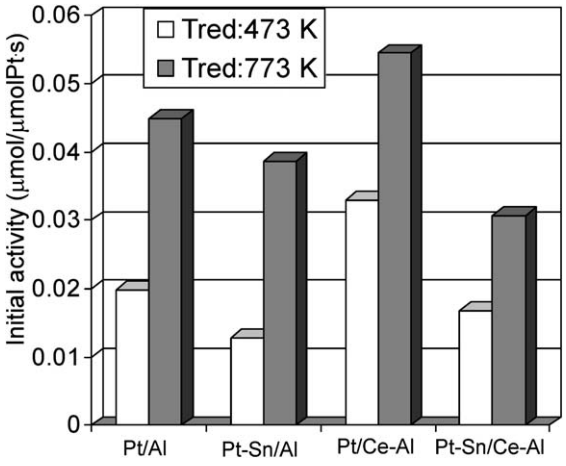

Fig. 8. Initial catalytic activity for crotonaldehyde hydrogenation at 353 K for catalysts after reduction at 473 or 773 K.

Fig. 8 shows the initial overall activity (μmol of crotonaldehyde reacted per μmol of platinum per s) of the catalysts under study at reduction temperatures of 473 and 773 K. The activity values are reported only when a carbon balance was achieved (i.e., once the amount of crotonaldehyde leaving the reactor matched that fed minus that transformed into products). For catalysts reduced at low temperature, the initial activity followed the order $Pt/CeO_2–Al_2O_3 > PtAl_2O_3 > Pt–Sn/CeO_2–Al_2O_3 > Pt–Sn/Al_2O_3$. Using the value of activity for unpromoted Pt/Al_2O_3 as a reference, the higher activity found in $Pt/CeO_2–Al_2O_3$ indicates that cerium was already able to promote platinum at even a low reduction temperature. However, tin decreased the initial activity, possibly due to the partial blocking of platinum sites by tin.

Reduction at 773 K produced an increase in the initial activity in all cases, with the initial activity decreasing in the following order: $Pt/CeO_2–Al_2O_3 > PtAl_2O_3 > Pt–Sn/Al_2O_3 > Pt–Sn/CeO_2–Al_2O_3$. For the unpromoted Pt/Al_2O_3 catalyst, the observed increase in activity after reduction at high temperature is probably not due to changes in particle size, because XPS results indicate a constant Pt/Al atomic ratio (Table 2) with reduction temperature. But the high-temperature reduction treatment changes the energetic distribution of platinum sites for CO adsorption (Fig. 6a). The higher homogeneity found in the heat-coverage profile for CO adsorption after reduction at 773 K could indicate a possible superficial redistribution of the platinum exposed faces from an open faces or steps after reduction at 473 K to a higher number of dense (111) faces more favorable for crotonaldehyde hydrogenation [42] at a reduction temperature of 773 K. Furthermore, platinum catalysts supported on nonreducible supports, like alumina and silica, undergo structural and chemical changes on reduction at ⩾773 K [43]. Koningsberger et al. [44] showed that the size of metal clusters in Pt/Al_2O_3 remained stable after reduction at 573 and 723 K but also noted important changes in electron d distribution of metal particles as measured by EXAFS. This shift in the d-band distribution after high-temperature reduction could account for the Pt/Al_2O_3 catalyst's enhanced catalytic activity.

For $Pt–Sn/Al_2O_3$, the observed promotional effect after reduction at high temperature could be related to either the formation of Pt–Sn alloys or the existence of oxidized tin on platinum particles ($Pt–SnO_x$). Mössbauer results indicate that after reduction at 773 K, 31% of the tin was alloyed with Pt, 62% of the Sn was in the Sn(II) state, and 7% of the Sn was in the Sn(IV) state (Table 3). One proposal for the promotional effect of Sn is that the oxidized metal species act as electrophilic or Lewis acid sites for the adsorption and activation of the C=O bond of crotonaldehyde, via the lone electron pair of the oxygen atom [45]. Therefore, the onset of new $Pt–SnO_x$ sites would explain the observed enhancement in activity during the first stages of reaction.

Another proposal for the effects of Sn is that the Sn(II) is associated with the alumina support, and the role of Sn is to form zero-valent PtSn alloy particles, which change the electronic properties of Pt and decrease the size of the surface Pt ensembles (i.e., diluting the Pt surface atoms by forming an alloy) [15,16]. Density functional studies of ethanol and acetic acid adsorption on Pt and Pt_3Sn alloys showed that the carbon in ethanol or acetic acid binds only to Pt surface sites, whereas the oxygen in ethanol or acetic acid binds to either Pt or Sn surface sites. This theory is also consistent with results of Jerdev et al., who observed that model Sn/Pt(111) surfaces formed PtSn alloys that were twice as active as Pt(111) surfaces for the hydrogenation of crotonaldehyde [46]. Jerdev et al. observed that oxidic Sn species were not stable under reaction conditions.

For $Pt/CeO_2–Al_2O_3$, the enhanced initial activity could involve two effects: the decoration of metal particles by partially reduced ceria and the creation of new sites at the metal–support interface that are effective for activation of the carbonyl bond. For the $Pt–Sn/CeO_2–Al_2O_3$ catalyst, the initial activity of the catalyst increased as the reduction temperature increased. Based on the characterization studies, the higher reduction temperature caused an increase in the amount of reduced cerium (leading to more decoration of the Pt particles) and an alloying of the Sn and Pt.

The products obtained under the conditions used in this study were butyraldehyde (formed by hydrogenation of the C=C bond), crotyl alcohol (but-2-en-ol, formed by hydrogenation of the carbonyl C=O bond), butanol (formed on hydrogenation of the primary products butyraldehyde and crotyl alcohol), and the light hydrocarbon butane (formed through butanol hydrogenation). The selectivity to crotyl alcohol (mol%) as a function of the time on stream at 353 K after reduction at both low (473 K) and high (773 K) temperature is plotted in Figs. 9 and 10. The selectivity to crotyl alcohol for catalysts reduced at 473 K decreased in the following order: $Pt–Sn/CeO_2–Al_2O_3 > Pt/CeO_2–Al_2O_3 \sim Pt–Sn/Al_2O_3 > PtAl_2O_3$. Reduction at high temperature produced an increase in selectivity to crotyl alcohol for all catalysts; however, this increase was more pronounced for the promoted catalysts. The selectivity to crotyl alcohol for catalysts reduced at 773 K decreased in the following order: $Pt–Sn/CeO_2–Al_2O_3 > Pt/CeO_2–Al_2O_3 \sim Pt–Sn/Al_2O_3 \gg PtAl_2O_3$.

Pt/Al_2O_3 exhibited a low selectivity toward crotyl alcohol (<8%), as was expected for the unpromoted catalyst (Fig. 9a),

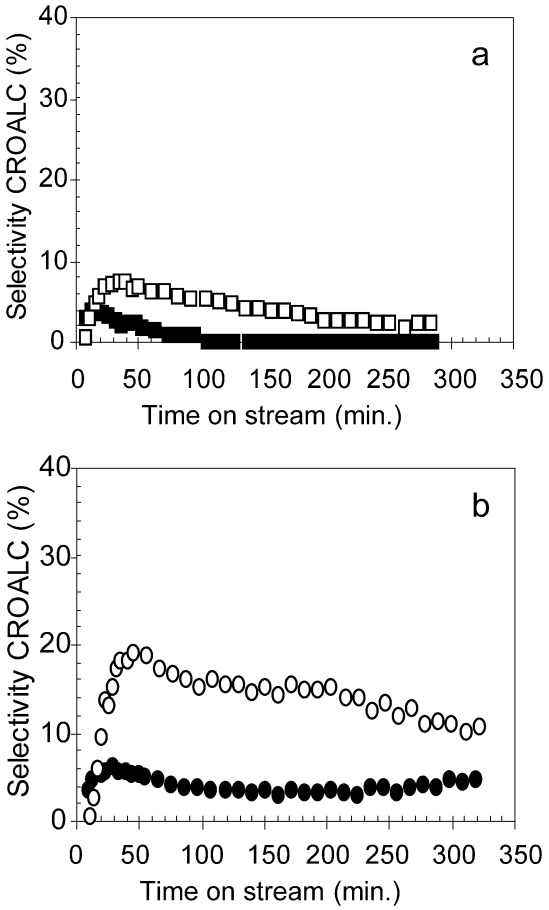

Fig. 9. Evolution of the selectivity toward crotyl alcohol as a function of the time on stream for the cerium-free catalysts at 353 K, after reduction at 473 (■, ●) or 773 K (□, ○). (a) Pt/Al_2O_3; (b) $Pt–Sn/Al_2O_3$.

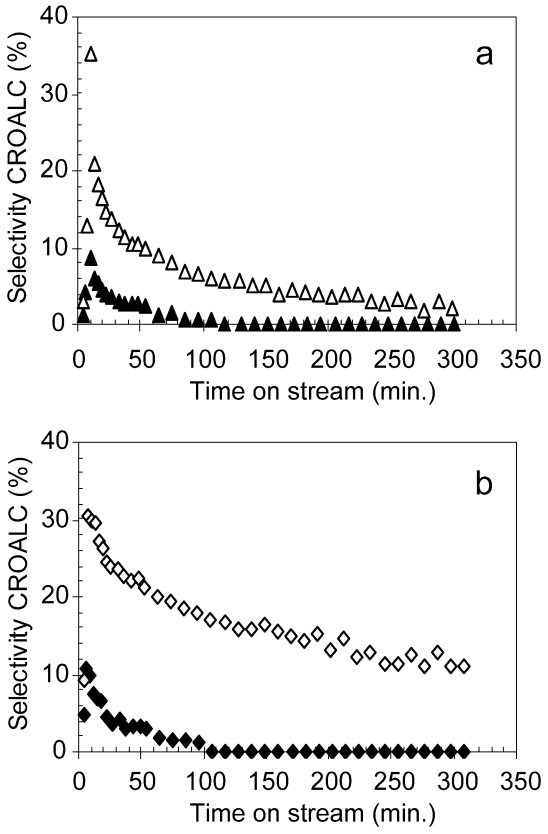

Fig. 10. Evolution of the selectivity toward crotyl alcohol as a function of the time on stream for the cerium-containing catalysts at 353 K, after reduction at 473 (solid symbols) or 773 K (open symbols). (a) $Pt/CeO_2–Al_2O_3$; (b) $Pt–Sn/CeO_2–Al_2O_3$.

and increasing the reduction temperature caused only a minor increase in crotyl alcohol selectivity. Reduction of this catalyst at 773 K caused some sintering, possibly resulting in a surface redistribution of platinum-exposed faces toward a higher number of (111) crystal planes. These close-packed metal faces are not favorable for the C=C coordination, and increased participation of these faces in the catalyst surface can improve the selectivity to crotyl alcohol [42].

For the promoted catalysts, $Pt–Sn–CeO_x$ interactions could modify the adsorption mode of crotonaldehyde on platinum particles. These interactions increased as the reduction temperature increased, as shown by XPS, microcalorimetry, and ^{119}Sn Mössbauer studies. DFT, microcalorimetry, and infrared studies of Pt and Pt_3Sn alloys with oxygenates indicated both an electronic and a geometric effect of adding Sn to Pt [31]. This modification also could explain the origin of the enhanced selectivity observed for the Sn-promoted catalysts for crotonaldehyde hydrogenation. A higher electronic density on platinum atoms creates a weaker interaction of the C=C bond of crotonaldehyde, favoring adsorption via the C=O bond and leading to increased selectivity toward crotyl alcohol [45]. This higher electron density is formed by the creation of PtSn, $Pt–SnO_x$, and $Pt–CeO_x$ (Pt decorated with CeO_x) sites that are able to activate the carbonyl bond of the crotonaldehyde molecule. Poisoning of these sites by strong adsorption of reactant and/or products would be the origin of the observed loss of selectivity with time on stream, which is also accompanied by the decrease in overall activity.

4. Conclusion

This study demonstrates that adding Sn (in a Pt/Sn 1:1 atomic ratio) and/or CeO_2 to Pt/Al_2O_3 catalysts improved the selectivity to crotyl alcohol during crotonaldehyde hydrogenation. Adding ceria to Pt/Al_2O_3 improved the initial activity for crotonaldehyde hydrogenation, whereas adding Sn (in the amount used in this study) to Pt/Al_2O_3 or $Pt/CeO_2–Al_2O_3$ decreased the catalytic activity. XPS and ^{119}Sn Mössbauer spectroscopy results showed that reduction of tin was partially inhibited by the presence of cerium. Moreover, the presence of tin facilitated the reduction of cerium. Reduction at 773 K decreased the number of platinum surface sites for the unpromoted and promoted catalysts. The decoration of platinum particles by patches of partially reduced ceria and oxidized tin species or formation of PtSn alloys can account for this loss. This effect produced the onset of new $Pt–CeO_x$, $Pt–SnO_x$, and PtSn sites, which would explain the observed change in activity for crotonaldehyde hydrogenation. These new sites can selectively interact with the C=O bond of the crotonaldehyde molecule, enhancing the selectivity toward crotyl alcohol.

Acknowledgments

Financial support by the Comisión Interministerial de Ciencia y Tecnología (Projects BQU 2000-0467 and BQU 2003-06150) is gratefully acknowledged. J.C.S.-R. also thanks the Ministerio de Educación y Ciencia (Spain) for a FPI grant. The authors also thank Dr. F. Coloma for helping with the XPS measurements.

References

[1] S.J. Tauster, S.C. Fung, R.L. Garten, J. Am. Chem. Soc. 100 (1978) 170.
[2] A. Dandekar, M.A. Vanicce, J. Catal. 183 (1999) 344.
[3] D.A. Aranda, M. Schmal, J. Catal. 171 (1997) 398.
[4] S. Bernal, J.J. Calvino, M.A. Cauqui, J.M. Gatica, C. Larese, J.A. Perez Omil, J.M. Pintado, Catal. Today 50 (1999) 175.
[5] S. Bernal, J.J. Calvino, M.A. Cauqui, J.M. Gatica, C. Lopez Cartes, J.A. Perez Omil, J.M. Pintado, Catal. Today 77 (2003) 385.
[6] A.K. Datye, D.S. Kalakkad, M.H. Yao, D.J. Smith, J. Catal. 155 (1995) 148.
[7] C.H. Bartholomew, R.B. Pannel, J.L. Butler, J. Catal. 65 (1980) 335.
[8] A. Sepúlveda-Escribano, F. Coloma, F. Rodríguez-Reinoso, J. Catal. 178 (1998) 649.
[9] J. Silvestre-Albero, F. Rodríguez-Reinoso, A. Sepúlveda-Escribano, J. Catal. 210 (2002) 127.
[10] M. Abid, G. Ehret, R. Touroude, Appl. Catal. A Gen. 217 (2001) 219.
[11] J.A. Dumesic, S.A. Stevenson, R.D. Sherwood, R.T.K. Baker, J. Catal. 99 (1986) 79.
[12] D.E. Resasco, R.J. Fenoglio, M.P. Suarez, J.O. Cechini, J. Phys. Chem. 90 (1986) 4330.
[13] S. Bernal, J.J. Calvino, J.M. Gatica, C. Larese, C. López-Cartes, J.A. Pérez-Omil, J. Catal. 169 (1997) 510.
[14] M. Abid, V.P. Boncour, R. Touroude, Appl. Catal. A Gen. 297 (2006) 48.
[15] R.D. Cortright, J.A. Dumesic, J. Catal. 148 (1994) 771.
[16] R.D. Cortright, J.M. Hill, J.A. Dumesic, Catal. Today 55 (2000) 213.
[17] A. Huidobro, A. Sepúlveda-Escribano, F. Rodríguez-Reinoso, J. Catal. 212 (2002) 94.
[18] F. Coloma, A. Sepúlveda-Escribano, J.L.G. Fierro, F. Rodríguez-Reinoso, Appl. Catal. A Gen. 136 (1996) 231.
[19] F. Coloma, A. Sepúlveda-Escribano, J.L.G. Fierro, F. Rodríguez-Reinoso, Appl. Catal. A Gen. 148 (1996) 63.
[20] B.E. Spiewak, J.A. Dumesic, Thermochim. Acta 290 (1996) 43.
[21] B. Riguetto, S. Damyanova, G. Goluliev, C. Marques, L. Petrov, J.M. Bueno, J. Phys. Chem. B 108 (2004) 5349.
[22] R.M. Navarro, M.C. Álvarez-Galván, M.C. Sánchez-Sánchez, F. Rosa, J. Fierro, Appl. Catal. B Environ. 55 (2005) 229.
[23] J.Z. Shyu, K. Otto, Appl. Surf. Sci. 32 (1998) 246.
[24] R. Bouwman, P. Biloen, J. Catal. 48 (1977) 209.
[25] M.J. Tiernan, O.E. Finlayson, Appl. Catal. B Environ. 19 (1998) 23.
[26] E. Merlen, P. Beuat, J.C. Bertolini, P. Delichère, N. Zanier, B. Didillon, J. Catal. 159 (1996) 178.
[27] Y. Weishen, L. Liwu, F. Yining, Z. Jingling, Catal. Lett. 12 (1992) 267.
[28] Y. Zhou, S.M. Davis, Catal. Lett. 15 (1992) 51.
[29] R. Bacaud, P. Bussiere, F. Figueras, J. Catal. 69 (1981) 399.
[30] M. Donders, B. Noorlander, D. van der Vliet, Bimetallics: Selective Hydrogenation, April 2004.
[31] R. Alcala, J.W. Shabaker, G.W. Huber, M.A. Sanchez-Castillo, J.A. Dumesic, J. Phys. Chem. B 109 (2005) 2074.
[32] G. Meizner, G. Via, F. Lytle, S. Fung, J. Sinfelt, J. Phys. Chem. 92 (1988) 2925.
[33] A. Caballero, H. Dexpert, B. Didillon, F. Lepeltier, O. Clause, J. Lynch, J. Phys. Chem. 97 (1993) 11283.
[34] C. Vértes, E. Tálas, I. Czakó-Nagy, J. Ryczkowski, S. Göbölos, A. Vértes, J. Margitfalvi, Appl. Catal. 68 (1991) 149.
[35] G. Del Angel, A. Bonilla, Y. Peña, J. Navarrete, J. Fierro, D.R. Acosta, J. Catal. 219 (2003) 63.
[36] A. Laachir, V. Perrichon, A. Badri, J. Lamotte, E. Catherine, J.C. Lavalley, J. El Fallal, L. Hilaire, F. le Normand, E. Quéméré, G.N. Sauvion, O. Touret, J. Chem. Soc. Faraday Trans. 87 (1991) 1601.
[37] M.S.P. Mastelaro, V.R. Nascente, A.O.A. Florentino, J. Phys. Chem. B 105 (2001) 10515.
[38] A. Guerrero-Ruiz, A. Maroto-Valiente, M. Cerro-Alarcón, B. Bachiller-Baeza, I. Rodriguez-Ramos, Top. Catal. 19 (2002) 303.
[39] H. Lieske, J. Volter, J. Catal. 90 (1984) 46.
[40] S.M. Stagg, C.A. Querini, W.E. Alvarez, D.E. Resasco, J. Catal. 168 (1997) 75.
[41] M. English, A. Jentys, J.A. Lercher, J. Catal. 166 (1997) 25.
[42] F. Delbeq, S. Sautet, J. Catal. 152 (1995) 217.
[43] G.J. den Otter, F.M. Dautzenberg, J. Catal. 53 (1978) 116.
[44] D.C. Koningsberger, M. Vaarkamp, Phys. B Condens. Matter 208–209 (1995) 633.
[45] P. Gallezot, D. Richard, Catal. Rev. Sci. Eng. 40 (1998) 81.
[46] D.I. Jerdev, A. Olivas, B.E. Koel, J. Catal. 205 (2002) 278.
[47] P. Beccat, J.C. Bertolini, Y. Gauthier, J. Massardier, P. Ruiz, J. Catal. 126 (1990) 451.